Generation and Reactivity of a $Ni^{III}_2(\mu$-1,2-peroxo) Complex

Norman Zhao, Alexander S. Filatov, Jiaze Xie, Ethan A. Hill, Andrey Yu. Rogachev, and John S. Anderson*

Department of Chemistry, University of Chicago, Chicago, Illinois 60637, United States

Department of Chemistry, Illinois Institute of Technology, Chicago, IL 60616, United States

Supporting Information Placeholder

ABSTRACT: High-valent transition metal-oxo, peroxo and superoxo complexes are crucial intermediates in processes including both biological and synthetic oxidation of organic substrates, water oxidation, as well as oxygen reduction. While high-valent oxygenated complexes of Mn, Fe, Co, and Cu are increasingly well known, high-valent oxygenated Ni complexes are comparatively rarer. Herein, we report the isolation of such an unusual high-valent species in a thermally-unstable $Ni^{III}_2(\mu$-1,2-peroxo) complex, which has been characterized using single-crystal X-ray diffraction and X-ray absorption, NMR, and UV-vis spectroscopies. Reactivity studies show that this complex is stable to dissociation of oxygen but is reactive with simple nucleophiles and electrophiles.

High-valent oxygenated transition metal species, such as oxo, peroxo, and superoxo complexes, are ubiquitous intermediates in oxidative reactivity. In particular, oxygenated first-row transition metal complexes are prominent in both biological and synthetic systems for the oxidation of organic substrates,[1,2] water oxidation,[3,4] and oxygen reduction.[5,6] Despite the generality of these proposed intermediates, the high reactivity of oxygenated transition metal complexes can make isolation and characterization challenging. Nevertheless, understanding their structure, properties, and viability is essential to elucidating or improving many processes.[7]

While numerous examples of high-valent oxygenated complexes of Mn,[8–14] Fe,[11,12,14–18] Co,[13,19–24] and Cu[25–33] have been isolated and studied, significantly fewer oxygenated Ni complexes have been reported.[13,34–49] This is despite the fact that high-valent Ni-oxo, peroxo, or superoxo complexes have been invoked in water oxidation,[50,51] biological superoxide dismutation,[52] oxygen reduction,[53] as well as organic oxidation catalysis.[35,40,54] No well-defined terminal Ni-oxo complexes are known, and Ni-superoxo species are still rare.[40,41,55,56] In the case of Ni-peroxo complexes, several examples of mononuclear Ni^{III} species have been reported,[57–60] and some dinuclear complexes have been transiently observed.[61,62] One $Ni^{II}_2(\mu$-1,2-peroxo) complex has recently been structurally characterized,[63] but no high-valent bridging Ni-peroxo complexes are known, despite the potential importance of these species in, for example, oxo coupling mechanisms for water oxidation by Ni-based layered double hydroxides.[50,51,64]

Previously, tris(NHC)phenylborate (NHC = N-heterocyclic carbene) ligands have been used to stabilize unusual Co^{III}-oxo and Fe^{III}-oxo complexes.[19,65] We rationalized that this system might also aid in the stabilization of high-valent Ni complexes with oxygen-based ligands. Herein, we report the use of $PhB(^tBuIm)_3^-$ to isolate the first example of a $Ni^{III}_2(\mu$-1,2-peroxo) complex $\{[PhB(^tBuIm)_3]Ni–O–O–Ni[(^tBuIm)_3BPh]\}\{BAr^F_4\}_2$ (**2**, BAr^F_4 = tetrakis(3,5-bis(trifluoromethyl)phenylborate). Complex **2** has been structurally characterized, and its properties have been examined using a variety of spectroscopic techniques. Reactivity studies show that **2** is comparatively stable to oxygen dissociation, C–H activation, and O-atom transfer, but reacts rapidly with both nucleophiles and electrophiles at low temperature. These results demonstrate that high-valent bridging Ni-peroxo intermediates are viable and provides insight into their properties and reactivity.

The synthesis of the Ni-chloride precursor $[PhB(^tBuIm)_3]NiCl$ (**1**) was recently reported by our group.[66] As **1** shows no reactivity under an atmosphere of oxygen for several days, we screened common halide abstractors such as Na^+, Ag^+, and Tl^+ salts to encourage reactivity. While addition of AgOTf or TlOTf led to intractable mixtures of diamagnetic products, treatment of **1** with $NaBAr^F_4$ in dichloromethane (DCM) causes the solution to change from dull chartreuse green to dark emerald green, indicative of the formation of a

Scheme 1. Synthesis of **1-Na** and **2**.

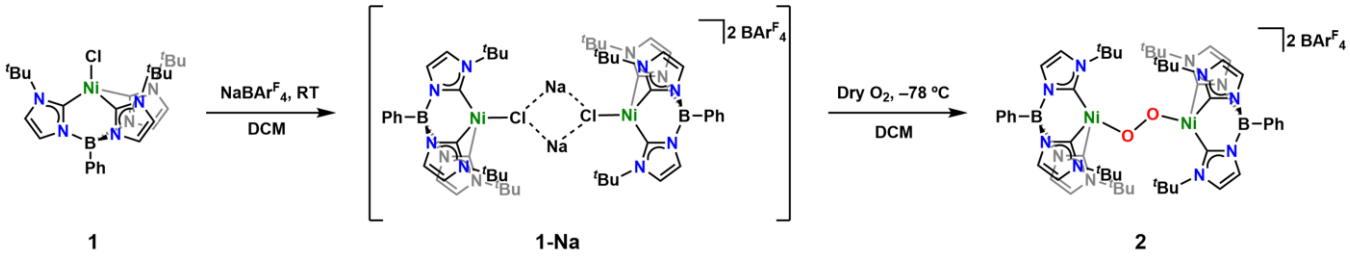

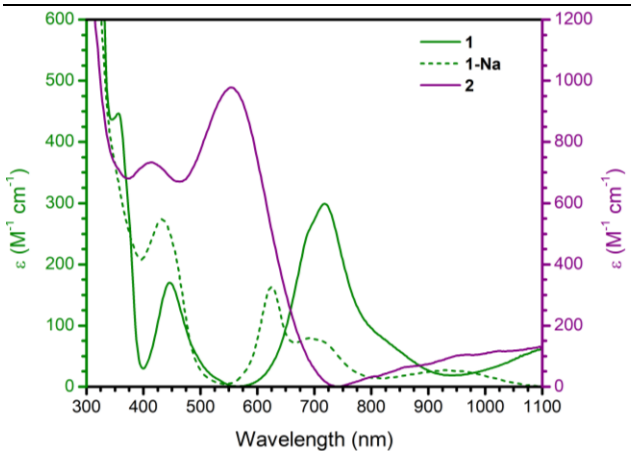

Figure 1. UV-vis spectra of **1**, **1-Na** (at RT) and **2** (at −78 °C) in DCM. Left y-axis is for **1** and **1-Na**, and right y-axis is for **2**.

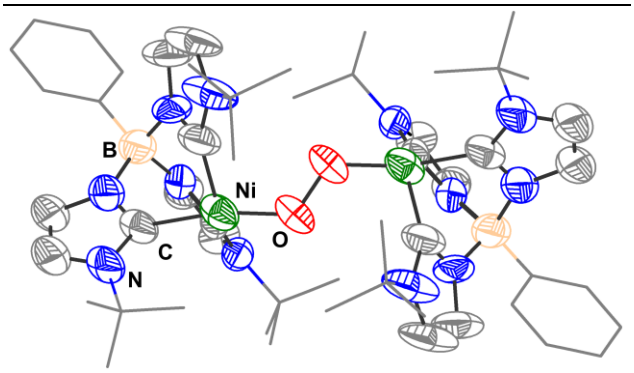

Figure 2. SXRD structure of **2**. Ni shown in green, oxygen in red, carbon in gray, nitrogen in blue and boron in tan. Ellipsoids shown at 50% probability. Solvent molecules, counterions and H-atoms omitted and parts of ligand scaffold shown as wireframe for clarity.

new species **1-Na** (Scheme 1, Figure 1). We found that a similar color change is observed in other non-coordinating solvents such as 1,3-difluorobenzene. However, **1-Na** is extremely sensitive to even small amounts of coordinating impurities such as ethers or variation in preparation conditions precluding detailed characterization of this species (Figure S1). While we do not have concrete characterization data on this complex, we tentatively propose an intermediate structurally similar to **1** with a weak interaction between Na^+ ions and the chloride ligand. This proposed structure is also supported by comparing the paramagnetic ^1H NMR spectra of **1** and **1-Na** that show a shifted, but similar overall pattern of resonances. Furthermore, treatment of **1-Na** with 12-*crown*-4 ether to sequester Na^+ ions regenerates **1** by ^1H NMR spectroscopy (Figure S2). Based on these data, and similar species previously reported, we tentatively propose that **1-Na** is a dimer as depicted in Scheme 1.[67]

Treatment of **1-Na** in DCM with dry oxygen at room temperature results in an intractable brown mixture of diamagnetic products as ascertained by ^1H NMR spectroscopy. However, at −78 °C addition of either stoichiometric or excess oxygen to **1-Na** in DCM results in a nearly instantaneous color change from emerald green to dark purple (Figure S3 and S4). We assign this new purple species as the dimeric Ni^{III}_2(μ-1,2-peroxo) complex {[PhB(^{t}BuIm)$_3$]Ni–O–O–Ni[(^{t}BuIm)$_3$BPh]}{BAr^F_4}$_2$, **2** (Scheme 1). The distinct color change is reflected in the UV-vis spectrum of **2** (Figure 1) displaying features at 410 nm (740 $M^{-1}cm^{-1}$) and 550 nm (970 $M^{-1}cm^{-1}$) which are dramatically different from those in **1** or **1-Na**. Time-dependent density functional theory calculations provide a reasonable reproduction of the electronic absorption spectrum, assigning the main feature at 550 nm to a mixed ligand-to-metal charge-transfer transition (Figure S5).

Fortunately, dark purple crystals of **2** can be grown over several days at −78 °C. Single- crystal X-ray diffraction (SXRD) confirms the formation of a Ni^{III}_2(μ-1,2-peroxo) complex (Figure 2). While the quality and resolution of the dataset is limited due to the crystal containing large numbers of solvent molecules and severe disorder of $BAr^F_4^-$ counterions, the structure of **2** nevertheless provides important information. The O–O bond length is 1.42(2) Å, which falls between the O–O bond length observed in Meyer's β-diketiminato Ni^{II}_2(μ-1,2-peroxo) complex (1.465(2) Å), and Nam's mononuclear η^2 12-TMC and 13-TMC Ni^{III}-peroxo complexes (12-TMC = 1,4,7,10-tetramethyl-1,4,7,10-tetraazacyclododecane, 13-TMC = 1,4,7,10-tetramethyl-1,4,7,10-tetraazacyclotridecane) (1.386(4) Å and 1.383(4) Å, respectively).[57,63] For comparison, the O–O bond lengths in two previously isolated Ni_2(μ-1,2-superoxo) complexes are 1.33 and 1.35 Å.[34,63] The spin density of **2** calculated by density functional theory (DFT) is primarily localized on Ni which further supports the formulation of this complex as a Ni^{III}_2(μ-1,2-peroxo) complex (Figure S5). The solid-state structure of **2** shows that the Ni^{III} centers adopt a seesaw geometry, with a Ni–O bond length of 1.796(9) Å and a Ni–O–O–Ni dihedral angle of 161.8(5)°. The Ni–O bond lengths are shorter than those of Meyer's Ni^{II}_2(μ-1,2-peroxo) complex, which has Ni–O bond lengths of 1.834(2) Å and a dihedral angle of 89.9(2)°.[63] The shorter Ni–O distances are consistent with a higher oxidation state of Ni^{III} in **2**.

A similar solution and solid-state structure of **2** is supported by NMR spectroscopic data. The ^1H NMR spectrum of **2** collected at −78 °C has broadened and shifted resonances, consistent with a paramagnetic species (Figure S6). In compound **1**, the ^1H NMR resonances (CD_2Cl_2) at 106 and 16 ppm have been assigned to the hydrogens of the imidazol-2-ylidene backbone. A similar pattern is seen in **2**, but with a doubling of these signals (118, 106, −13, −17 ppm), suggestive of an asymmetric dimer at −78 °C. Additionally, two large resonances corresponding to the *tert*-butyl groups are visible at 15 and 17 ppm. We propose this pattern arises from a combination of the seesaw geometry about the nickel centers and slow isomerization about the B–Ni–O vector at −78 °C, as observed in a Ni-methyl complex supported by this ligand scaffold.[66] The same ^1H NMR spectra are observed for samples of crystalline **2** dissolved in CD_2Cl_2 and samples of **2** generated *in situ* by addition of O_2 to **1-Na**, confirming that complex **2** is formed *in situ* in a relatively clean manner.

The effective magnetic moment of **2** was measured by Evans' method at −78 °C to be μ_{eff} = 3.2(1) μ_B. This value is higher than would be expected for two weakly coupled S = 1/2 centers ($\mu_{S.O.}$ = 2.45 μ_B) but is more consistent with ferromagnetic coupling to give an S = 1 ground state ($\mu_{S.O.}$ = 2.82 μ_B). DFT calculations support this assignment, predicting a ferromagnetically coupled system (J = 36 cm^{-1}), and showing spin density consistent with ferromagnetic exchange (Figure S5). Additionally, the X-band electron paramagnetic resonance spectrum of a solution of **2** in DCM at 15 K is nearly silent, with only a weak signal centered around g = 2 accounting for <10%

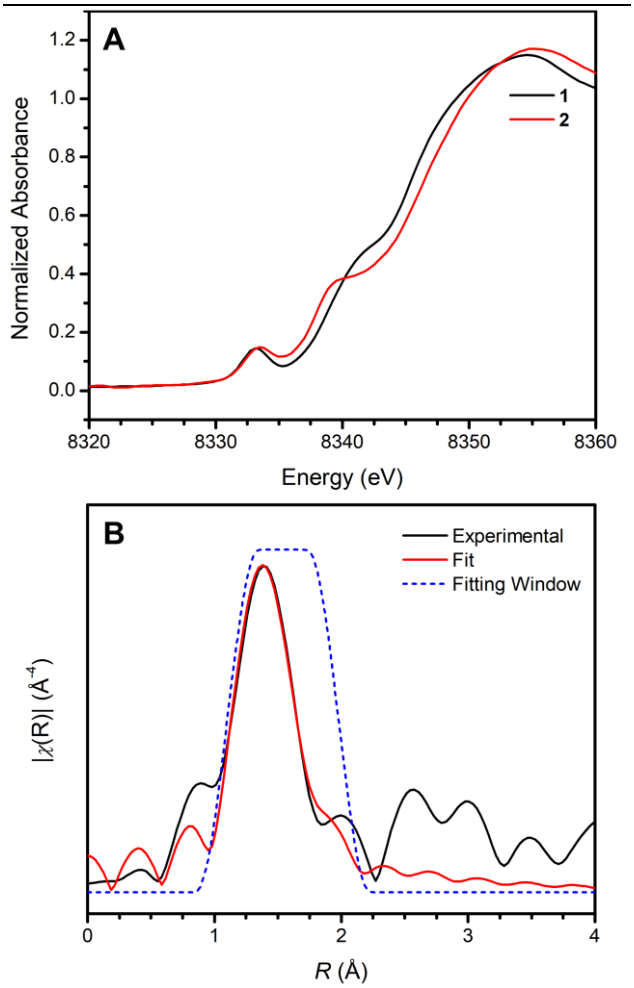

Figure 3. (A) Ni K-edge X-ray absorption of **1** and **2**, showing the normalized energies of the X-ray absorption near edge structure (XANES) region. (B) EXAFS (black) and fit (red) in R-space at the Ni K-edge absorption of **2**.

of the Ni in the sample by spin integration. While metal complexes bridged by dioxygen ligands are commonly antiferromagnetically coupled, there is a recent example of a ferromagnetically coupled copper system.[68] While we are unable to perform solid-state magnetometry on **2** due to its thermal instability, we have acquired variable-temperature Evans' method measurements. An accurate determination of the *J* coupling constant is not possible due to a limited temperature range from the solvent freezing point and compound stability, but a persistent moment of ~3 μ_B further supports the assigned $S = 1$ ground state (Figure S7).

To further interrogate the solution-state structure of **2**, and probe the assigned oxidation states of Ni, we turned to Ni K-edge X-ray absorption spectroscopy (XAS). The Ni K-edge of **2** (8346.1 eV, THF frozen solution, –135 °C) occurs at higher energy relative to **1** (8345.4 eV, powder, room temperature) (Figure 3A, S8 and S9, and Table S1). The difference in the Ni K-edge between **1** and **2** is outside of error (±0.4 eV), but it should be noted that one-electron oxidation from Ni^{II} to Ni^{III} in synthetic complexes produces shifts ranging from 0 to 1.8 eV and care must therefore be taken in interpreting this shift as an indicator of oxidation state change.[35,57,69,70] Analysis of the extended X-ray absorption fine structure (EXAFS) region of **2** suggests a reasonable fit with a simple model containing one oxygen and three carbon atoms in the first shell, consistent with the structure obtained by SXRD (Figure 3B and S10 and Table S2). Taken together, the observed bond lengths, magnetic properties, and shift in the Ni K-edge of **2** support the assignment of a $Ni^{III}_2(\mu$-1,2-peroxo) complex.

We synthesized the $^{18}O_2$ isotopologue of **2** to further characterize the O–O bond through vibrational spectroscopy. However, we were unable to assign a vibrational band to the O–O stretch by either infrared or Raman spectroscopy of **2** at low temperatures, likely due to either Raman laser photodegradation of **2** or weak resonance enhancement of the peroxo vibration (Figure S11).[37]

With complex **2** in hand, we sought to examine its reactivity, particularly the possible reversibility of dioxygen binding as this process has relevance to oxygen evolution. Subjecting **2** to several freeze-pump-thaw cycles in DCM resulted in no change in the UV-vis spectrum of the solution. This observation excludes an equilibrium process for O_2 binding. Additionally, **2** does not react with dihydroanthracene or phosphines at low temperature. However, addition of 10 equivalents of tetrabutylammonium chloride (TBACl) to **2** in DCM at –78 °C produced a color change from dark purple to green upon warming to –50 °C and 87% recovery of **1** was observed by ^{1}H NMR spectroscopy (Figure S12 and S13). The balanced reaction requires the formal release of O_2, however, we have not been able to observe dioxygen release into the headspace by GC analysis under the reaction conditions. We hypothesize that a short-lived reactive oxygen species (ROS) or Ni complex must be generated that reacts further in solution. However, we have been unable to definitively intercept any such species using a variety of reagents including the singlet oxygen trap 9,10-dimethylanthracene or the ROS trap 1,3-diphenylisobenzofuran.[71]

To investigate alternative reactivity, we next treated **2** with trimethylsilyl chloride (TMSCl), hypothesizing that oxygen could be released in the form of bis(trimethylsilyl) peroxide (TMS_2O_2). Instead, addition of 10 equivalents of TMSCl to **2** at –78 °C yields bis(trimethylsilyl) ether (TMS_2O) by ^{1}H NMR and GC-MS in good yield. Complex **1** was not observed in this reaction mixture. Addition of TMSCl to ^{18}O-labeled **2** followed by GC-MS analysis confirms that the oxygen in the resultant TMS_2O arises from **2** (Figure S14). We propose that any TMS_2O_2 formed in the reaction is decomposed by reactive Ni-containing products. Indeed, TMS_2O_2 that was added concomitantly with TMSCl to **2** under the same reaction conditions is decomposed. Despite these complicated product distributions, the observed reactivity suggests that this $Ni^{III}_2(\mu$-1,2-peroxo) complex does not release oxygen dissociatively and instead reacts with other species such as nucleophiles or electrophiles.

In summary, we have generated and characterized an unusual $Ni^{III}_2(\mu$-1,2-peroxo) complex, **2**. The SXRD structure, along with X-ray absorption, ^{1}H NMR and UV-vis spectra of **2** confirm the assignment of a $Ni^{III}_2(\mu$-1,2-peroxo) moiety. Furthermore, this complex is reactive towards both nucleophiles, such as Cl^-, and electrophiles, such as TMSCl. Taken together, these data demonstrate that $Ni^{III}_2(\mu$-1,2-peroxo) species are synthetically accessible and provide insights into their reactivity.

ASSOCIATED CONTENT

Supporting Information

The Supporting Information is available free of charge on the ACS Publications website.

- Materials, methods, compound characterization and-supplementary figures and tables
- DFT optimized geometries for complex **2**
- Crystallographic Information File (CIF)

AUTHOR INFORMATION

Corresponding Author

jsanderson@uchicago.edu
John S. Anderson

Notes

The authors declare no competing financial interests.

ACKNOWLEDGMENT

Work presented here was funded by the following sources:
This work was supported by an NSF CAREER award (Grant No. 1654144). JSA also gratefully acknowledges support from the Sloan Research Foundation (FG-2019-11497) and 3M Corporation through an NTFA. NZ is supported by the National Science Foundation Graduate Research Fellowship (DGE-1746045). Financial support from the ACS Petroleum Research Fund to AYuR (60838-ND6) is gratefully acknowledged. MRCAT operations are supported by the Department of Energy and the MRCAT member institutions. This research used resources of the Advanced Photon Source, a U.S. Department of Energy (DOE) Office of Science User Facility operated for the DOE Office of Science by Argonne National Laboratory under Contract No. DE-AC02-06CH11357. We thank Dr. Mark Warren, Dr. Joshua Wright and Dr. John Katsoudas for assistance with XAS data acquisition at beamline 10-BM-A,B. We also thank John Hack (UChicago), Ida DiMucci (Cornell), Prof. Kyle Lancaster (Cornell), Ryan Hall (UW-Madison), Laura Elmendorf (UW-Madison) and Prof. Thomas Brunold (UW-Madison) for helpful discussions about vibrational spectroscopy, and Prof. Jonathan Rittle for helpful discussions on the reactivity of the Ni-peroxo complex.

REFERENCES

(1) Yee, G. M.; Tolman, W. B. Transition Metal Complexes and the Activation of Dioxygen BT - Sustaining Life on Planet Earth: Metalloenzymes Mastering Dioxygen and Other Chewy Gases; Kroneck, P. M. H., Sosa Torres, M. E., Eds.; Springer International Publishing: Cham, 2015; pp 131–204.

(2) Engelmann, X.; Monte-Pérez, I.; Ray, K. Oxidation Reactions with Bioinspired Mononuclear Non-Heme Metal–Oxo Complexes. *Angew. Chem. Int. Ed.* **2016**, *55*, 7632–7649.

(3) Askerka, M.; Brudvig, G. W.; Batista, V. S. The O2-Evolving Complex of Photosystem II: Recent Insights from Quantum Mechanics/Molecular Mechanics (QM/MM), Extended X-Ray Absorption Fine Structure (EXAFS), and Femtosecond X-Ray Crystallography Data. *Acc. Chem. Res.* **2017**, *50*, 41–48.

(4) Hunter, B. M.; Gray, H. B.; Müller, A. M. Earth-Abundant Heterogeneous Water Oxidation Catalysts. *Chem. Rev.* **2016**, *116*, 14120–14136.

(5) Pegis, M. L.; Wise, C. F.; Martin, D. J.; Mayer, J. M. Oxygen Reduction by Homogeneous Molecular Catalysts and Electrocatalysts. *Chem. Rev.* **2018**, *118*, 2340–2391.

(6) Gewirth, A. A.; Varnell, J. A.; DiAscro, A. M. Nonprecious Metal Catalysts for Oxygen Reduction in Heterogeneous Aqueous Systems. *Chem. Rev.* **2018**, *118*, 2313–2339.

(7) Vicens, L.; Olivo, G.; Costas, M. Rational Design of Bioinspired Catalysts for Selective Oxidations. *ACS Catal.* **2020**, *10*, 8611–8631.

(8) Kovacs, J. A. Tuning the Relative Stability and Reactivity of Manganese Dioxygen and Peroxo Intermediates via Systematic Ligand Modification. *Acc. Chem. Res.* **2015**, *48*, 2744–2753.

(9) Neu, H. M.; Baglia, R. A.; Goldberg, D. P. A Balancing Act: Stability versus Reactivity of Mn(O) Complexes. *Acc. Chem. Res.* **2015**, *48*, 2754–2764.

(10) Kanady, J. S.; Mendoza-Cortés, J. L.; Goddard III, W. A.; Agapie, T. *Oxygen-Evolving Complex of Photosystem II: Insights from Computation and Synthetic Models*; CRC Press: United States, North America, 2015.

(11) Baglia, R. A.; Zaragoza, J. P. T.; Goldberg, D. P. Biomimetic Reactivity of Oxygen-Derived Manganese and Iron Porphyrinoid Complexes. *Chem. Rev.* **2017**, *117*, 13320–13352.

(12) Larson, V. A.; Battistella, B.; Ray, K.; Lehnert, N.; Nam, W. Iron and Manganese Oxo Complexes, Oxo Wall and Beyond. *Nat. Rev. Chem.* **2020**, *4*, 404–419.

(13) Fiedler, A. T.; Fischer, A. A. Oxygen Activation by Mononuclear Mn, Co, and Ni Centers in Biology and Synthetic Complexes. *J. Biol. Inorg. Chem.* **2017**, *22*, 407–424.

(14) Battistella, B.; Ray, K. O_2 and H_2O_2 Activations at Dinuclear Mn and Fe Active Sites. *Coord. Chem. Rev.* **2020**, *408*, 213176.

(15) Nam, W. Synthetic Mononuclear Nonheme Iron–Oxygen Intermediates. *Acc. Chem. Res.* **2015**, *48*, 2415–2423.

(16) Lu, X.; Li, X.-X.; Lee, Y.-M.; Jang, Y.; Seo, M. S.; Hong, S.; Cho, K.-B.; Fukuzumi, S.; Nam, W. Electron-Transfer and Redox Reactivity of High-Valent Iron Imido and Oxo Complexes with the Formal Oxidation States of Five and Six. *J. Am. Chem. Soc.* **2020**, *142*, 3891–3904.

(17) Oswald, V. F.; Lee, J. L.; Biswas, S.; Weitz, A. C.; Mittra, K.; Fan, R.; Li, J.; Zhao, J.; Hu, M. Y.; Alp, E. E.; Bominaar, E. L.; Guo, Y.; Green, M. T.; Hendrich, M. P.; Borovik, A. S. Effects of Noncovalent Interactions on High-Spin Fe(IV)–Oxido Complexes. *J. Am. Chem. Soc.* **2020**, *142*, 11804–11817.

(18) Drummond, M. J.; Ford, C. L.; Gray, D. L.; Popescu, C. V; Fout, A. R. Radical Rebound Hydroxylation Versus H-Atom Transfer in Non-Heme Iron(III)-Hydroxo Complexes: Reactivity and Structural Differentiation. *J. Am. Chem. Soc.* **2019**, *141*, 6639–6650.

(19) Goetz, M. K.; Hill, E. A.; Filatov, A. S.; Anderson, J. S. Isolation of a Terminal Co(III)-Oxo Complex. *J. Am. Chem. Soc.* **2018**, *140*, 13176–13180.

(20) Kumar, P.; Lindeman, S. V; Fiedler, A. T. Cobalt Superoxo and Alkylperoxo Complexes Derived from Reaction of Ring-Cleaving Dioxygenase Models with O_2. *J. Am. Chem. Soc.* **2019**, *141*, 10984–10987.

(21) Corona, T.; Padamati, S. K.; Acuña-Parés, F.; Duboc, C.; Browne, W. R.; Company, A. Trapping of Superoxido Cobalt and Peroxido Dicobalt Species Formed

Reversibly from Co^{II} and O_2. *Chem. Commun.* **2017**, *53*, 11782–11785.

(22) Tcho, W.-Y.; Wang, B.; Lee, Y.-M.; Cho, K.-B.; Shearer, J.; Nam, W. A Mononuclear Nonheme Cobalt(III)–Hydroperoxide Complex with an Amphoteric Reactivity in Electrophilic and Nucleophilic Oxidative Reactions. *Dalton Trans.* **2016**, *45*, 14511–14515.

(23) Kim, D.; Cho, J.; Lee, Y.-M.; Sarangi, R.; Nam, W. Synthesis, Characterization, and Reactivity of Cobalt(III)–Oxygen Complexes Bearing a Macrocyclic N-Tetramethylated Cyclam Ligand. *Chem. Eur. J.* **2013**, *19*, 14112–14118.

(24) Jo, Y.; Annaraj, J.; Seo, M. S.; Lee, Y.-M.; Kim, S. Y.; Cho, J.; Nam, W. Reactivity of a Cobalt(III)-Peroxo Complex in Oxidative Nucleophilic Reactions. *J. Inorg. Biochem.* **2008**, *102*, 2155–2159.

(25) Elwell, C. E.; Gagnon, N. L.; Neisen, B. D.; Dhar, D.; Spaeth, A. D.; Yee, G. M.; Tolman, W. B. Copper–Oxygen Complexes Revisited: Structures, Spectroscopy, and Reactivity. *Chem. Rev.* **2017**, *117*, 2059–2107.

(26) Fukuzumi, S.; Karlin, K. D. Kinetics and Thermodynamics of Formation and Electron-Transfer Reactions of $Cu–O_2$ and $Cu_2–O_2$ Complexes. *Coord. Chem. Rev.* **2013**, *257*, 187–195.

(27) Gagnon, N.; Tolman, W. B. $[CuO]^+$ and $[CuOH]_2^+$ Complexes: Intermediates in Oxidation Catalysis? *Acc. Chem. Res.* **2015**, *48*, 2126–2131.

(28) Dahl, E. W.; Dong, H. T.; Szymczak, N. K. Phenylamino Derivatives of Tris(2-Pyridylmethyl)Amine: Hydrogen-Bonded Peroxodicopper Complexes. *Chem. Commun.* **2018**, *54*, 892–895.

(29) Kim, B.; Jeong, D.; Cho, J. Nucleophilic Reactivity of Copper(II)–Alkylperoxo Complexes. *Chem. Commun.* **2017**, *53*, 9328–9331.

(30) Iovan, D. A.; Wrobel, A. T.; McClelland, A. A.; Scharf, A. B.; Edouard, G. A.; Betley, T. A. Reactivity of a Stable Copper–Dioxygen Complex. *Chem. Commun.* **2017**, *53*, 10306–10309.

(31) Kindermann, N.; Günes, C.-J.; Dechert, S.; Meyer, F. Hydrogen Atom Abstraction Thermodynamics of a μ-1,2-Superoxo Dicopper(II) Complex. *J. Am. Chem. Soc.* **2017**, *139*, 9831–9834.

(32) Isaac, J. A.; Thibon-Pourret, A.; Durand, A.; Philouze, C.; Le Poul, N.; Belle, C. High-Valence $Cu^{II}Cu^{III}$ Species in Action: Demonstration of Aliphatic C–H Bond Activation at Room Temperature. *Chem. Commun.* **2019**, *55*, 12711–12714.

(33) Large, T. A. G.; Mahadevan, V.; Keown, W.; Stack, T. D. P. Selective Oxidation of Exogenous Substrates by a Bis-Cu(III) Bis-Oxide Complex: Mechanism and Scope. *Inorganica Chim. Acta* **2019**, *486*, 782–792.

(34) Shiren, K.; Ogo, S.; Fujinami, S.; Hayashi, H.; Suzuki, M.; Uehara, A.; Watanabe, Y.; Moro-oka, Y. Synthesis, Structures, and Properties of Bis(μ-Oxo)Nickel(III) and Bis(μ-Superoxo)Nickel(II) Complexes: An Unusual Conversion of a $Ni^{III}_2(\mu\text{-}O)_2$ Core into a Ni^{II}_2 $\mu\text{-}OO)_2$ Core. *J. Am. Chem. Soc.* **2000**, *122*, 254–262.

(35) Corona, T.; Draksharapu, A.; Padamati, S. K.; Gamba, I.; Martin-Diaconescu, V.; Acuña-Parés, F.; Browne, W. R.; Company, A. Rapid Hydrogen and Oxygen Atom Transfer by a High-Valent Nickel–Oxygen Species. *J. Am. Chem. Soc.* **2016**, *138*, 12987–12996.

(36) Corona, T.; Company, A. Spectroscopically Characterized Synthetic Mononuclear Nickel–Oxygen Species. *Chem. Eur. J.* **2016**, *22*, 13422–13429.

(37) Fujita, K.; Schenker, R.; Gu, W.; Brunold, T. C.; Cramer, S. P.; Riordan, C. G. A Monomeric Nickel–Dioxygen Adduct Derived from a Nickel(I) Complex and O_2. *Inorg. Chem.* **2004**, *43*, 3324–3326.

(38) Noh, H.; Cho, J. Synthesis, Characterization and Reactivity of Non-Heme 1st Row Transition Metal-Superoxo Intermediates. *Coord. Chem. Rev.* **2019**, *382*, 126–144.

(39) Hikichi, S.; Yoshizawa, M.; Sasakura, Y.; Akita, M.; Moro-Oka, Y. First Synthesis and Structural Characterization of Dinuclear M(III) Bis(μ-Oxo) Complexes of Nickel and Cobalt with Hydrotris(Pyrazolyl)Borate Ligand. *J. Am. Chem. Soc.* **1998**, *120*, 10567–10568.

(40) Padamati, S. K.; Angelone, D.; Draksharapu, A.; Primi, G.; Martin, D. J.; Tromp, M.; Swart, M.; Browne, W. R. Transient Formation and Reactivity of a High-Valent Nickel(IV) Oxido Complex. *J. Am. Chem. Soc.* **2017**, *139*, 8718–8724.

(41) McNeece, A. J.; Jesse, K. A.; Xie, J.; Filatov, A. S.; Anderson, J. S. Generation and Oxidative Reactivity of a Ni(II) Superoxo Complex via Ligand-Based Redox Non-Innocence. *J. Am. Chem. Soc.* **2020**, *142*, 10824–10832.

(42) Morimoto, Y.; Takagi, Y.; Saito, T.; Ohta, T.; Ogura, T.; Tohnai, N.; Nakano, M.; Itoh, S. A Bis(μ-Oxido)Dinickel(III) Complex with a Triplet Ground State. *Angew. Chem. Int. Ed.* **2018**, *57*, 7640–7643.

(43) Cho, J.; Furutachi, H.; Fujinami, S.; Tosha, T.; Ohtsu, H.; Ikeda, O.; Suzuki, A.; Nomura, M.; Uruga, T.; Tanida, H.; Kawai, T.; Tanaka, K.; Kitagawa, T.; Suzuki, M. Sequential Reaction Intermediates in Aliphatic C-H Bond Functionalization Initiated by a Bis(μ-Oxo)Dinickel(III) Complex. *Inorg. Chem.* **2006**, *45*, 2873–2885.

(44) Cramer, S. P.; Brunold, T. C.; Mandimutsira, B. S.; Riordan, C. G.; Yamarik, J. L.; Gu, W.; Brunold, T. C.; Gu, W.; Cramer, S. P.; Riordan, C. G. Dioxygen Activation by a Nickel Thioether Complex: Characterization of a $Ni^{III}_2(\mu\text{-}O)_2$ Core. *J. Am. Chem. Soc.* **2002**, *123*, 9194–9195.

(45) Itoh, S.; Bandoh, H.; Nagatomo, S.; Kitagawa, T.; Fukuzumi, S. Aliphatic Hydroxylation by a Bis(μ-Oxo)Dinickel(III) Complex. *J. Am. Chem. Soc.* **1999**, *121*, 8945–8946.

(46) Honda, K.; Cho, J.; Matsumoto, T.; Roh, J.; Furutachi, H.; Tosha, T.; Kubo, M.; Fujinami, S.; Ogura, T.; Kitagawa, T.; Suzuki, M. Oxidation Reactivity of Bis(μ-Oxo) Dinickel(III) Complexes: Arene Hydroxylation of the Supporting Ligand. *Angew. Chem. Int. Ed.* **2009**, *48*, 3304–3307.

(47) Kieber-Emmons, M. T.; Annaraj, J.; Seo, M. S.; Van Heuvelen, K. M.; Tosha, T.; Kitagawa, T.; Brunold, T. C.; Nam, W.; Riordan, C. G. Identification of an "End-on" Nickel–Superoxo Adduct, $[Ni(Tmc)(O_2)]^+$. *J. Am. Chem. Soc.* **2006**, *128*, 14230–14231.

(48) Nagataki, T.; Tachi, Y.; Itoh, S. Ni^{II}(TPA) as an Efficient Catalyst for Alkane Hydroxylation with m-CPBA.

Chem. Commun. **2006**, *0*, 4016–4018.

(49) Yao, S.; Bill, E.; Milsmann, C.; Wieghardt, K.; Driess, M. A "Side-on" Superoxonickel Complex [LNi(O_2)] with a Square-Planar Tetracoordinate Nickel(II) Center and Its Conversion into [LNi(μ-OH)$_2$NiL]. *Angew. Chem. Int. Ed.* **2008**, *47*, 7110–7113.

(50) Li, N.; Bediako, D. K.; Hadt, R. G.; Hayes, D.; Kempa, T. J.; von Cube, F.; Bell, D. C.; Chen, L. X.; Nocera, D. G. Influence of Iron Doping on Tetravalent Nickel Content in Catalytic Oxygen Evolving Films. *Proc. Natl. Acad. Sci. U.S.A.* **2017**, *114*, 1486–1491.

(51) Lee, S.; Banjac, K.; Lingenfelder, M.; Hu, X. Oxygen Isotope Labeling Experiments Reveal Different Reaction Sites for the Oxygen Evolution Reaction on Nickel and Nickel Iron Oxides. *Angew. Chem. Int. Ed.* **2019**, *58*, 10295–10299.

(52) Barondeau, D. P.; Kassmann, C. J.; Bruns, C. K.; Tainer, J. A.; Getzoff, E. D. Nickel Superoxide Dismutase Structure and Mechanism. *Biochemistry* **2004**, *43*, 8038–8047.

(53) Vij, V.; Sultan, S.; Harzandi, A. M.; Meena, A.; Tiwari, J. N.; Lee, W.-G. G.; Yoon, T.; Kim, K. S. Nickel-Based Electrocatalysts for Energy-Related Applications: Oxygen Reduction, Oxygen Evolution, and Hydrogen Evolution Reactions. *ACS Catal.* **2017**, *7*, 7196–7225.

(54) Morimoto, Y.; Bunno, S.; Fujieda, N.; Sugimoto, H.; Itoh, S. Direct Hydroxylation of Benzene to Phenol Using Hydrogen Peroxide Catalyzed by Nickel Complexes Supported by Pyridylalkylamine Ligands. *J. Am. Chem. Soc.* **2015**, *137*, 5867–5870.

(55) Fukuzumi, S.; Lee, Y.-M.; Nam, W. Structure and Reactivity of the First-Row d-Block Metal-Superoxo Complexes. *Dalton Trans.* **2019**, *48*, 9469–9489.

(56) Corona, T.; Pfaff, F. F.; Acuña-Parés, F.; Draksharapu, A.; Whiteoak, C. J.; Martin-Diaconescu, V.; Lloret-Fillol, J.; Browne, W. R.; Ray, K.; Company, A. Reactivity of a Nickel(II) Bis(Amidate) Complex with Meta-Chloroperbenzoic Acid: Formation of a Potent Oxidizing Species. *Chem. Eur. J.* **2015**, *21*, 15029–15038.

(57) Cho, J.; Sarangi, R.; Annaraj, J.; Kim, S. Y.; Kubo, M.; Ogura, T.; Solomon, E. I.; Nam, W. Geometric and Electronic Structure and Reactivity of a Mononuclear 'Side-on' Nickel(III)–Peroxo Complex. *Nat. Chem.* **2009**, *1*, 568–572.

(58) Cho, J.; Kang, H. Y.; Liu, L. V.; Sarangi, R.; Solomon Cd, E. I.; Nam, W.; Solomon, E. I.; Nam, W. Mononuclear Nickel(II)-Superoxo and Nickel(III)-Peroxo Complexes Bearing a Common Macrocyclic TMC Ligand. *Chem. Sci.* **2013**, *4*, 1502–1508.

(59) Yao, S.; Xiong, Y.; Vogt, M.; Grützmacher, H.; Herwig, C.; Limberg, C.; Driess, M. O-O Bond Activation in Heterobimetallic Peroxides: Synthesis of the Peroxide [LNi(μ,H2:H2-O2)K] and Its Conversion into a Bis(μ-Hydroxo) Nickel Zinc Complex. *Angew. Chem. Int. Ed.* **2009**, *48*, 8107–8110.

(60) Matsumoto, M.; Nakatsu, K. Dioxygen-Bis-t-Butylisocyanide)Nickel. *Acta Crystallogr. Sect. B* **1975**, *31*, 2711–2713.

(61) Kieber-Emmons, M. T.; Schenker, R.; Yap, G. P. A.; Brunold, T. C.; Riordan, C. G. Spectroscopic Elucidation of a Peroxo Ni$_2$(μ-O$_2$) Intermediate Derived from a Nickel(I) Complex and Dioxygen. *Angew. Chem. Int. Ed.* **2004**, *43*, 6716–6718.

(62) Rettenmeier, C. A.; Wadepohl, H.; Gade, L. H. Structural Characterization of a Hydroperoxo Nickel Complex and Its Autoxidation: Mechanism of Interconversion between Peroxo, Superoxo, and Hydroperoxo Species. *Angew. Chem. Int. Ed.* **2015**, *54*, 4880–4884.

(63) Duan, P.-C.; Manz, D.-H.; Dechert, S.; Demeshko, S.; Meyer, F. Reductive O_2 Binding at a Dihydride Complex Leading to Redox Interconvertible μ-1,2-Peroxo and μ-1,2-Superoxo Dinickel(II) Intermediates. *J. Am. Chem. Soc.* **2018**, *140*, 4929–4939.

(64) Martirez, J. M. P.; Carter, E. A. Unraveling Oxygen Evolution on Iron-Doped β-Nickel Oxyhydroxide: The Key Role of Highly Active Molecular-like Sites. *J. Am. Chem. Soc.* **2019**, *141*, 693–705.

(65) Smith, J. M.; Mayberry, D. E.; Margarit, C. G.; Sutter, J.; Wang, H.; Meyer, K.; Bontchev, R. P. N–O Bond Homolysis of an Iron(II) Tempo Complex Yields an Iron(III) Oxo Intermediate. *J. Am. Chem. Soc.* **2012**, *134*, 6516-6519.

(66) Hill, E. A.; Zhao, N.; Filatov, A. S.; Anderson, J. S. Nickel(II)-Methyl Complexes Adopting Unusual Seesaw Geometries. *Chem. Commun.* **2020**, *56*, 7861-7864.

(67) Holze, P.; Corona, T.; Frank, N.; Braun-Cula, B.; Herwig, C.; Company, A.; Limberg, C. Activation of Dioxygen at a Lewis Acidic Nickel(II) Complex: Characterization of a Metastable Organoperoxide Complex. *Angew. Chem. Int. Ed.* **2017**, *56*, 2307–2311.

(68) Kindermann, N.; Bill, E.; Dechert, S.; Demeshko, S.; Reijerse, E. J.; Meyer, F. A Ferromagnetically Coupled (S = 1) Peroxodicopper(II) Complex. *Angew. Chem. Int. Ed.* **2015**, *54*, 1738–1743.

(69) Colpas, G. J.; Maroney, M. J.; Bagyinka, C.; Kumar, M.; Willis, W. S.; Suib, S. L.; Mascharak, P. K.; Baidya, N. X-Ray Spectroscopic Studies of Nickel Complexes, with Application to the Structure of Nickel Sites in Hydrogenases. *Inorg. Chem.* **1991**, *30*, 920–928.

(70) Mondal, P.; Pirovano, P.; Das, A.; Farquhar, E. R.; McDonald, A. R. Hydrogen Atom Transfer by a High-Valent Nickel-Chloride Complex. *J. Am. Chem. Soc.* **2018**, *140*, 1834–1841.

(71) Greer, A. Christopher Foote's Discovery of the Role of Singlet Oxygen [$^1O_2$ ($^1\Delta_g$)] in Photosensitized Oxidation Reactions. *Acc. Chem. Res.* **2006**, *39*, 797–804.

SYNOPSIS TOC (Word Style "SN_Synopsis_TOC"). If you are submitting your paper to a journal that requires a synopsis graphic and/or synopsis paragraph, see the Instructions for Authors on the journal's homepage for a description of what needs to be provided and for the size requirements of the artwork.

To format double-column figures, schemes, charts, and tables, use the following instructions:

Place the insertion point where you want to change the number of columns
From the **Insert** menu, choose **Break**
Under **Sections**, choose **Continuous**
Make sure the insertion point is in the new section. From the **Format** menu, choose **Columns**
In the **Number of Columns** box, type **1**
Choose the **OK** button

Now your page is set up so that figures, schemes, charts, and tables can span two columns. These must appear at the top of the page. Be sure to add another section break after the table and change it back to two columns with a spacing of 0.33 in.

Table 1. Example of a Double-Column Table

Column 1	Column 2	Column 3	Column 4	Column 5	Column 6	Column 7	Column 8

Authors are required to submit a graphic entry for the Table of Contents (TOC) that, in conjunction with the manuscript title, should give the reader a representative idea of one of the following: A key structure, reaction, equation, concept, or theorem, etc., that is discussed in the manuscript. Consult the journal's Instructions for Authors for TOC graphic specifications.